Final Report for AOARD Grant FA2386-12-1-4023

"**Photoresponsive liquid crystals: Fundamental study and applications**"

2013/03/08

Name of Principal Investigators (PI and Co-PIs):
PI: Vincent K. S. Hsiao
 – e-mail address : kshsiao@ncnu.edu.tw
 – Institution : National Chi Nan University
 – Mailing Address : No.1, University Rd., Puli, Nantou, Taiwan, 54561
 – Phone : +886-49-2910960 ext4907
 – Fax : +886-49-2912238
Co-PI: Chih-Chien Chu
 – e-mail address : jrchu3933@gmail.com
 – Institution : Chung Shan Medical University
 – Mailing Address : No 110, Sec. 1, Jianguo N.Rd., Taichung City,Taiwan, 40421
 – Phone : +886-4-24730022 ext. 12227
 – Fax : +886-4-23248189

Period of Performance: 3/5/2012 – 3/4/2013

Abstract: The final report summarizes the works done under the support from AOARD project number: FA2386-12-1-4023. The report starts from the optical characterization of the photoresponsive liquid crystals (LCs) consisting of newly synthesized azobenzene molecules dispersed in nematic LCs. The report also contains our new finding of the optically switchable fluorescent properties of studied azobenzene molecules alone and in the azobenzene-impregnated porous silicon. Finally we describe our recent works on using those photoresponsive LC in two-dimensional (2D) gratings and subwavelength gratings which have potential use in spectroscopic applications. The outcomes of the project end with three published publications and two submitted papers.

Introduction: LCs have been successfully employed in various photonic devices, such as LC laser, that have demonstrated superiority over other conventional inorganic or organic materials. Recently, the tremendous progress of laser technology has made the study of light-matter interaction easier. For example, the birefringence of LC could be switched by light stimulus by doping photoresponsive molecules, such as azobenzene derivatives, into LCs or synthesize an inherently photoresponsive LC. The use of light as external stimulus to switch or align the LC phases has several advantages because such process could be carried in rapid and precise manner under a high degree of a spatial control. azobenzenes are very attractive to study in the light-driven experiments, since their photoisomerization (trans→cis) is considered as a cleanest photochemical process. In the final report here, we present our one-year study on azobenzene molecules and used them in the photoactive photonic structures. From the AOARD project support, we have achieved to synthesis new azobenzene molecule which can lower the cleaning temperature nematic LC host. The finding could be considered alternative ways to achieve light-tunable LC by thermal effect. The most exciting findings are that we realize the optically tunable photoluminescence (PL) properties of studied azobenzene and also discover an interesting result where the PL is optically switchable in the

Report Documentation Page		*Form Approved* *OMB No. 0704-0188*
Public reporting burden for the collection of information is estimated to average 1 hour per response, including the time for reviewing instructions, searching existing data sources, gathering and maintaining the data needed, and completing and reviewing the collection of information. Send comments regarding this burden estimate or any other aspect of this collection of information, including suggestions for reducing this burden, to Washington Headquarters Services, Directorate for Information Operations and Reports, 1215 Jefferson Davis Highway, Suite 1204, Arlington VA 22202-4302. Respondents should be aware that notwithstanding any other provision of law, no person shall be subject to a penalty for failing to comply with a collection of information if it does not display a currently valid OMB control number.		

1. REPORT DATE **13 MAR 2013**	2. REPORT TYPE **Final**	3. DATES COVERED **05-03-2012 to 04-03-2013**

4. TITLE AND SUBTITLE **Photoresponsive Liquid Crystals: Fundamental Study and Applications**	5a. CONTRACT NUMBER **FA23861214023**
	5b. GRANT NUMBER
	5c. PROGRAM ELEMENT NUMBER
6. AUTHOR(S) **Kuei-Sen Hsiao**	5d. PROJECT NUMBER
	5e. TASK NUMBER
	5f. WORK UNIT NUMBER
7. PERFORMING ORGANIZATION NAME(S) AND ADDRESS(ES) **National Chi Nan University,No 1 University Rd Puli,Nantou Hsien 54561,Taiwan,NA,NA**	8. PERFORMING ORGANIZATION REPORT NUMBER **N/A**
9. SPONSORING/MONITORING AGENCY NAME(S) AND ADDRESS(ES) **AOARD, UNIT 45002, APO, AP, 96338-5002**	10. SPONSOR/MONITOR'S ACRONYM(S) **AOARD**
	11. SPONSOR/MONITOR'S REPORT NUMBER(S) **AOARD-124023**

12. DISTRIBUTION/AVAILABILITY STATEMENT **Approved for public release; distribution unlimited**

13. SUPPLEMENTARY NOTES

14. ABSTRACT

The report starts from the optical characterization of the photoresponsive liquid crystals (LCs) consisting of newly synthesized azobenzene molecules dispersed in nematic LCs. The report also contains the new finding of the optically switchable fluorescent properties of studied azobenzene molecules alone and in the azobenzene-impregnated porous silicon. Finally The PI describes his recent work on using those photoresponsive LC in two-dimensional (2D) gratings and subwavelength gratings which have potential use in spectroscopic applications.

15. SUBJECT TERMS **Liquid Crystals, Photonic Devices, Display Technologies**

16. SECURITY CLASSIFICATION OF:			17. LIMITATION OF ABSTRACT	18. NUMBER OF PAGES	19a. NAME OF RESPONSIBLE PERSON
a. REPORT **unclassified**	b. ABSTRACT **unclassified**	c. THIS PAGE **unclassified**	**Same as Report (SAR)**	**22**	

Standard Form 298 (Rev. 8-98)
Prescribed by ANSI Std Z39-18

azobenzene-impregnated porous silicon materials. Finally, we make 2D gratings and subwavelength gratings using holographic polymer-dispersed LC (H-PDLC) technique. Those gratings have potentials in spectroscopic applications.

Experiment: Please refer to the attached paper publications.

Results and Discussion:

1. Optical characteristics of newly synthesized azobenzene molecules (the work was not yet submitted to any journal)

We analyze the newly synthesized azo-molecules and characterize their ability to lower the cleaning temperature of cholesteric LCs (CLCs). We found out A4 can lower the cleaning temperature down to 35 degree, as shown in Fig.1. The effect was used in the optically switchable AQ dye doped LC system in which AQ dye absorbs the laser power and changes the phase [1]. We have successfully proved that A4 molecules could effectively change the CLC phase under 660 nm laser light illumination, as shown in Fig. 2. The controlled experiments have been down (not showing here) to prove the effect of light-induced switching in CLC need A4 and AQ dye together.
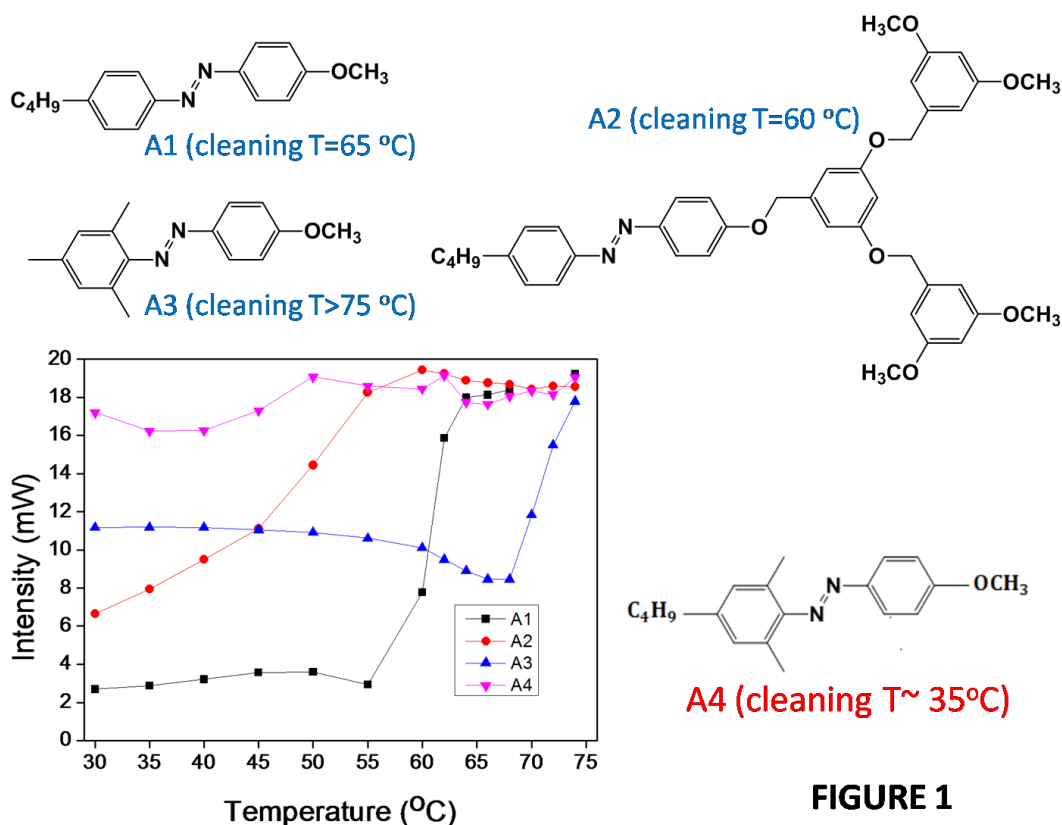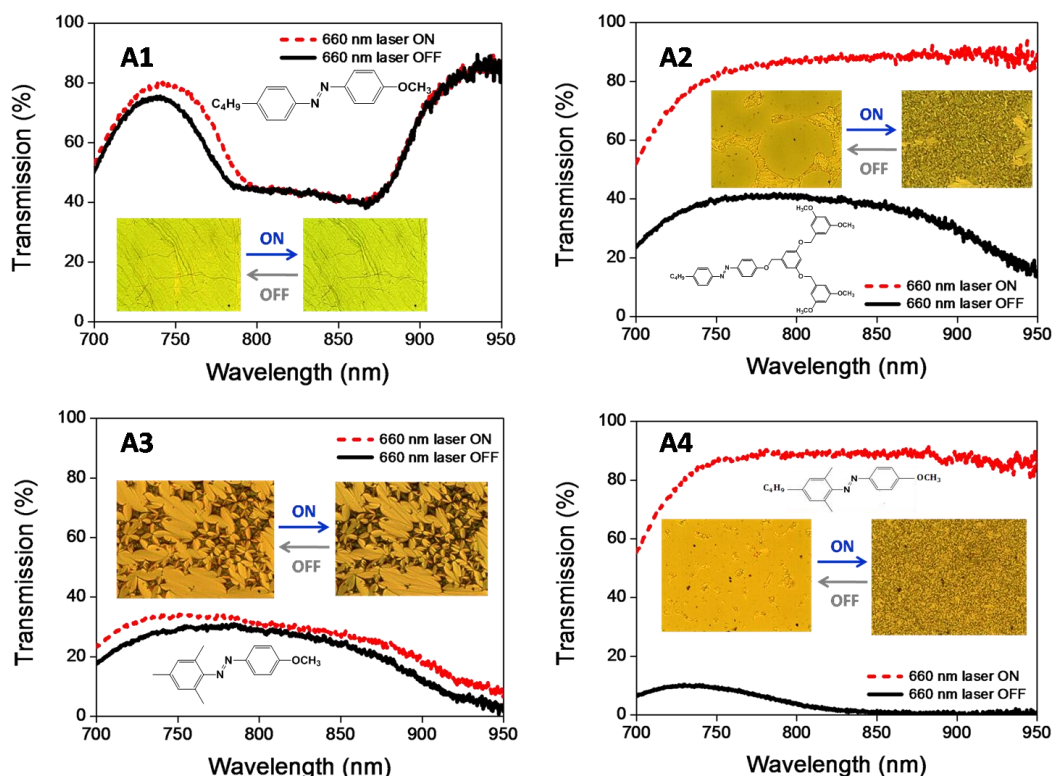

FIGURE 1

FIGURE 2

2. Photoswitchable fluorescence on/off behavior between cis- and trans-rich azobenzenes (the work has been published in Journal of Materials Chemistry)

We report rapid photoswitchable fluorescence on/off behavior between cis- and trans-rich 4-butyl-40-methoxyazobenzene and its analogue 4-butyl-2,6-dimethyl-4-methoxyazobenzene.
More details please refer to reference [2]

3. Light-induced spectral shifting generated from azo-dye doped holographic 2D gratings (the work has been published in Journal of Materials Chemistry)

Optically tunable two-dimensional (2D) gratings were holographically fabricated in azobenzene-doped polymer-dispersed liquid crystals using a single diffractive element. Our experiments showed that the diffraction efficiency of the gratings could be switched reversibly upon light irradiation. More importantly, we demonstrated for the first time that the diffractive spectrum from the holographic 2D gratings could be optically tuned about 24 nm, which might be useful for optically switchable filters and spectroscopic applications. The dynamic switching is attributed to the changes of refractive index modulation between LC-rich and polymer-rich areas due to the trans- cis-isomerization-triggered nematic- isotropic phase transition of liquid crystals. In addition, our 2D holographic gratings have polarization-insensitive optical properties for normally incident light. The all-optical tuning behavior is highly reversible and reproducible, making such kind of gratings promising in active photonic elements.
More details please refer to reference [3]

4. Large-angle color dispersion based on 2-D hexagonal subwavelength holographic gratings (the work has been published in IEEE Photonics journal)

This paper presents large-angle color dispersion using a holographically fabricated two dimensional (2D) subwavelength transmission grating. A dispersion angle of 68o is observed within continuous spectrum dispersion from 360 to 700 nm at an incident angle of 20o using white light as a probe beam. By changing the angle between the sample normal and the probe beam, the dispersed spectrum can be tuned at a spectral resolution of 3.6 nm per degree.
More details please refer to reference [4]

5. Reversibly light-modulated photoluminescence from azobenzene-impregnated porous silicon (the work was submitted to Journal of Materials Chemistry C)

Azobenzene-impregnated porous silicon (Azo-PS) was used, for the first time, as color-rewritable organic/inorganic hybrid material. Under UV light illumination, the generation of cis-Azo enhances the red photoluminescence (PL) emission. Images can be written and erased under external light and thermal stimulus.
More details please refer to reference [5]

List of Publications and Significant Collaborations that resulted from your AOARD supported project:

a) Papers published in peer-reviewed journals
1. B. -K. Tsai, C. -H. Chen, C. -H. Hung, **Vincent K. S. Hsiao**, C. -C. Chu*, " Photoswitchable fluorescence on/off behavior between cis- and trans-rich azobenzenes" *Journal of Materials Chemistry*, 22, 20874 (2012). (SCI, **IF = 5.968**)
2. Y. J. Liu, Y. -C. Su, Y. -J. Hsu, **Vincent K. S. Hsiao***, " Light-induced spectral shifting generated from azo-dye doped holographic 2D gratings" *Journal of Materials Chemistry*, 22, 14191 (2012). (SCI, **IF = 5.968**)
3. Y. -Y. Lo, J. Yu, Y. -C. Su, **Vincent K. S. Hsiao***, Z. Chen, " Large-angle color dispersion based on 2D hexagonal subwavelength holographic gratings" *IEEE Photonics Journal*, 5, 2220504 (2013). (SCI, **IF = 2.320**)

b) Manuscripts submitted but not yet published
1. Sheng-Lin Chen, Chih-Chien Chu and Vincent K. S. Hsiao* "Reversibly light-modulated photoluminescence from azobenzene-impregnated porous silicon", submitted to JMCC.

c) Interactions with industry or with Air Force Research Laboratory scientists or significant collaborations that resulted from this work.
We thank AFRL scientist, Timothy J. Bunning, for the helpful discussions and supports of nanostructured images. During the project period, we also establish collaborations with Professor Tzu-Chau Lin at Department of Chemistry in National Central University. We are trying to synthesis azobenzene based molecules which have light-controllable two photon absorption or fluorescence.

References:

1. L. V. Natarajan, T. J. White, J. M. Wofford, V. P. Tondiglia, R. L. Sutherland, S. A. Siwecki and T. J. Bunning, "Laser initiated thermal tuning of a cholesteric liquid crystal" Appl. Phys. Lett. 97, 011107 (2010)
2. B. -K. Tsai, C. -H. Chen, C. -H. Hung, **Vincent K. S. Hsiao**, C. -C. Chu∗, " Photoswitchable fluorescence on/off behavior between cis- and trans-rich azobenzenes" *Journal of Materials Chemistry*, 22, 20874 (2012). (SCI, **IF = 5.968**)
3. Y. J. Liu, Y. -C. Su, Y. -J. Hsu, **Vincent K. S. Hsiao∗**, " Light-induced spectral shifting generated from azo-dye doped holographic 2D gratings" *Journal of Materials Chemistry*, 22, 14191 (2012). (SCI, **IF = 5.968**)
4. Y. -Y. Lo, J. Yu, Y. -C. Su, **Vincent K. S. Hsiao∗**, Z. Chen, " Large-angle color dispersion based on 2D hexagonal subwavelength holographic gratings" *IEEE Photonics Journal*, 5, 2220504 (2013). (SCI, **IF = 2.320**)
5. Sheng-Lin Chen, Chih-Chien Chu and Vincent K. S. Hsiao∗ "Reversibly light-modulated photoluminescence from azobenzene-impregnated porous silicon", submitted to JMCC.

Attachments:
Reference 2-5

Reference 2

Journal of Materials Chemistry

COMMUNICATION

Photoswitchable fluorescence on/off behavior between *cis*- and *trans*-rich azobenzenes†

Bo-Kai Tsai,[a] Chien-Hong Chen,[a] Cheng-Hsiang Hung,[a] Vincent K. S. Hsiao[b] and Chih-Chien Chu[*ac]

We report rapid photoswitchable fluorescence on/off behavior between *cis*- and *trans*-rich 4-butyl-4′-methoxyazobenzene and its analogue 4-butyl-2,6-dimethyl-4′-methoxyazobenzene.

Azobenzene (Az) groups are typically used in a broad range of photochromic molecules that undergo rapid *trans/cis* reversible isomerization by switching the irradiation beam between UV and visible light.[1] Therefore, the incorporation of Az moieties into various functional materials was explored intensively during the previous decade to develop intelligent photoresponsive molecular systems for sensing, optical switching, and image-storing applications.[2] The molecular conformation of *trans*-Az isomers is rod-like, and they can be used as a photoresponsive calamitic liquid crystal (LC) mesogen or as the photochromic guest for host LC molecules.[3] Moreover, introducing a flexible alkyl chain and a polar group onto the 4,4′-positions of the two benzene rings also imparts liquid crystallinity for the Az scaffold, favoring molecular assembly through π–π stacking between the aromatic rings and van der Waals interactions between the alkyl chains, and increasing the compatibility with host LCs.
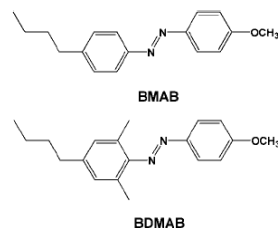
The characteristic π–π* (UV region) and n–π* (visible region) transitions corresponding to the *trans*- and *cis*-rich states, respectively, allow rapid scanning of photoswitchable behavior using UV-visible (UV-Vis) spectroscopy. However, it is known that they are incapable of emitting fluorescence with appreciable quantum yield upon UV light irradiation, despite the intense absorption of Az derivatives in the UV region.[4] Recently, Han and Hara reported intense fluorescence from light-driven self-assembled spherical aggregates of nonionic Az derivatives;[5] they have further demonstrated color-tunable fluorescence of a series of Az compounds containing electron-donating and -withdrawing pendant groups.[6] The authors proposed that this unusual fluorescence phenomenon was attributed to the aggregation-induced emission (AIE) and that only

the bent-shaped *cis*-isomers with a larger dipole moment favored the formation of head-to-tail intermolecular J-aggregates.[7,8]

According to the previous finding, it is noticed that fluorescent Az-based aggregates continued to show a *trans* ↔ *cis* photo-isomerization; however, their fluorescence expression was unaffected upon switching between UV and visible light irradiation. In other words, once the light-driven AIE was saturated, a reversible photo-isomerization process did not alter the emission intensity. In contrast, this communication provides unprecedented results of photo-switchable fluorescence behavior of 4-butyl-4′-methoxyazobenzene (BMAB),[9] a widely used LC azo guest, and its structural analogue 4-butyl-2,6-dimethyl-4′-methoxyazobenzene (BDMAB, Scheme 1).

The newly designed BDMAB bearing two methyl groups *ortho* to the azo moiety could reduce the coplanarity of the Az-conjugated system.[10] Therefore, compared with BMAB, BDMAB has slightly blue-shifted π–π* (from 350 to 338 nm) and red-shifted n–π* (from 434 to 446 nm) maximum absorption wavelengths. Moreover, *ortho*-dimethylation significantly reduces the rate of thermal *cis*-to-*trans* relaxation, efficiently retaining the longer lifetime of *cis* BDMAB.[11] On the basis of Han *et al.*'s assumption, the long-term stability of the *cis*-Az isomer has a potentially crucial function in producing aggregation-induced fluorescence.[12]

Initially, both *trans*- and *cis*-BMAB solution were non-fluorescent upon excitation at UV 365 nm. Following the previous procedure for generating observable fluorescence of *cis*-rich Az derivatives, *trans*-BMAB solution (5×10^{-4} M in THF) was then continuously exposed to UV light (365 nm, 100 W) for 30 min.[5] The UV-Vis absorption spectra shown in Fig. 1 exhibit a significant decrease of π–π* transition at 350 nm and an increase of n–π* transition at

[a]School of Applied Chemistry, Chung Shan Medical University, Taichung City 40201, Taiwan. E-mail: jrchu@csmu.edu.tw; Fax: +886-4-23248189
[b]Department of Applied Materials and Optoelectronic Engineering, National Chi Nan University, Puli, Nantou County 54561, Taiwan
[c]Department of Medical Education, Chung Shan Medical University Hospital, Taichung City 40201, Taiwan

† Electronic supplementary information (ESI) available: Experimental details including the synthesis and preparation of fluorescent azo compounds. Additional TEM images, UV-Vis absorption and fluorescence spectra. See DOI: 10.1039/c2jm34776h
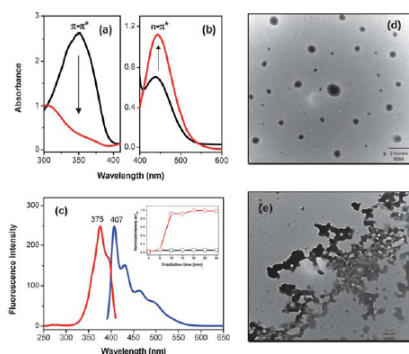
Scheme 1 Structures of the mesogen-like azobenzene derivatives.

20874 | *J. Mater. Chem.*, 2012, **22**, 20874–20877

This journal is © The Royal Society of Chemistry 2012

Fig. 1 UV-Vis spectra of UV-exposed BMAB solution. The change in absorbance of (a) π–π* and (b) n–π* transition. (c) Excitation (red line) and emission spectra (blue line) of *cis*-rich BMAB solution (5×10^{-4} M in THF); inset: time-dependent fluorescence intensity increase. TEM images of BMAB before (d) and after (e) UV light irradiation.

445 nm, which suggests a *cis*-rich photostationary state (PSS). Although the BMAB solution was dominated by the *cis*-isomers when exposed to UV light, its fluorescence intensity remained negligible. An unexpected blue fluorescence gradually increased as the solution was agitated gently over the UV light irradiation, and the intensity was rapidly saturated within 10 min (see ESI†). Fig. 1c shows the excitation, emission, and time-dependent intensity increase profiles for BMAB, and the obtained quantum yield referring to the standard was 0.036.[13] Additionally, an identical preparation method also produced the rapid fluorescence enhancement of the *cis*-rich BDMAB solution, suggesting that these two azo compounds possessed similar *trans*-to-*cis* photoisomerization kinetics and molecular assembly behavior in their *cis*-rich PSS states, regardless of the dimethyl groups at the *ortho* position.

Because the formation of ordered aggregated structures is critical to this fluorescence behavior, appropriate shaking during UV light exposure appears to have assisted the ordered molecular assembly pattern of *cis*-isomers. The UV light-driven fluorescence for *cis*-rich BMAB and BDMAB could be readily performed in various organic solvent systems, including THF, chloroform, toluene, and hexane, although the emission intensity increase in ethanol and DMF was minor. The observed solvent effect implies that a less-polar environment favors the assembly of azo molecules, and the consequent fluorescence intensity could increase significantly. Moreover, Fig. 1d and e, and Fig. S1† (higher magnification) show the TEM micrographs of BMAB before and after UV exposure, confirming the light-driven assembly of BMAB particles in the submicron dimension.

The ^{1}H NMR analyses (Fig. S2†) show that no structural decomposition or additional photoreaction of the Az unit (6.5–8.0 ppm) and the alkyl chain (0.5–2.8 ppm) occurs during UV light irradiation, and the ratio of *cis*- and *trans*-isomers in the UV light PSS can be determined by calculating the integral areas of the methoxy protons in each state. The NMR data estimate approximately 75% and 94% of *cis*-BMAB and *cis*-BDMAB isomers, respectively, in the UV-exposed solutions, confirming that *cis*-Az was the primary component for generating light-driven fluorescence. Moreover,

BDMAB solution containing 7% of *cis*-isomers initially showed greater *trans*-to-*cis* photoisomerization efficiency than BMAB solution, indicating relatively greater stability of the *ortho*-disubstituted Az compounds in the *cis* state.

Visible light irradiation causes rapid *cis*-to-*trans* isomerization of Az compounds, and thus, the *trans/cis* states for pristine BMAB and BDMAB could be reversibly switched by alternating UV and visible light irradiation. A reversible photoisomerization reaction of the fluorescent BMAB solution was also conducted using a handheld UV lamp (365 nm, 4 W) and white light bulb irradiation within 3 min to achieve *cis*- and *trans*-rich PSS, respectively. The change in maximum absorbance for n–π* transition confirms the *trans* ↔ *cis* photoisomerization by alternating the irradiation light source (Fig. S3†). Furthermore, the photo-induced *cis*-to-*trans* back reaction regenerated approximately 83% of *trans*-BMAB, and 43% of *trans*-BDMAB, indicating that BDMAB favors the relatively stable *cis* state even following light irradiation.

Because Az compound fluorescence correlates highly with *cis*-isomer content, it is anticipated that the fluorescence intensity can also be reversibly switched by alternating irradiation light sources to adjust the *trans*- and *cis*-contents in the system. However, Han and co-workers only observed a steady fluorescence expression when the *trans* and *cis* states of Az derivatives were switched. In sharp contrast, the emission intensity of fluorescent BMAB and BDMAB decreased significantly when exposed to white light irradiation, and then increased to the original magnitude when irradiated with UV light (Fig. S4†). Fig. 2 shows the visualized images of this unprecedented photoswitchable fluorescence "on/off" behavior of BMAB and the repeating cycles of switchable fluorescence accompanied by the *trans* ↔ *cis* photoisomerization monitored by the absorbance change of the n–π* transition. Because the two switched cycles correlate well, the *cis*-contents in the PSS dominates the change of the observed fluorescence intensity. Although the detailed mechanism for this
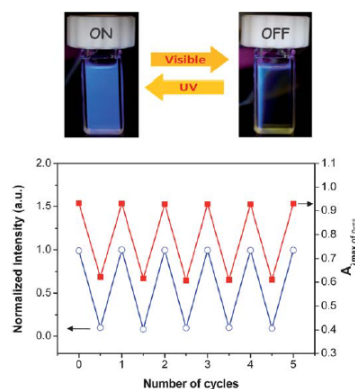

Fig. 2 The visualized images of photoswitchable fluorescence "on/off" behavior of BMAB and the repeating cycles of switchable fluorescence intensity (blue line) and *trans* ↔ *cis* photoisomerization (red line), monitored by fluorescence and UV-Vis absorption analyses, respectively. The fluorescence intensity was integrated from 400 to 700 nm.

fluorescence behavior is not well established, we proposed that the formation of intermolecular aggregation of *cis*-isomers is a dynamic process, in which the *trans*-isomers that are back generated by visible light irradiation trigger the disassembly of the aggregated structures. Therefore, the AIE phenomenon of azo compounds diminishes temporarily until the next UV irradiation cycle. Additionally, BDMAB solution that showed similar photoswitchable fluorescence maintained moderate emission levels following white light irradiation, whereas BMAB was almost non-fluorescent. The difference in the PSS of visible light between these two azo compounds is ascribed to the relatively abundant *cis*-content of BDMAB, allowing the partial retention of the assembled structure and the AIE.

Alternatively, *cis*-to-*trans* isomerization can also be carried out using thermal treatment following two possible mechanisms: simple rotation around the N–N bond or inversion through an sp-hybridized transition state.[14] On the basis of the decrease in the absorbance of the n–π* transition at ambient temperature (Fig. 3a), fitting the experimental data to the first-order kinetics produced a thermal relaxation rate and the half-life of *cis*-BMAB of 5.76×10^{-2} h^{-1} and approximately 12 h, respectively.[15] Conversely, *cis*-BDMAB was extremely stable in the dark, and the thermal back isomerization was significantly slower at room temperature. Presumably, the introduction of methyl groups on the two *ortho* positions restricts the rotation or the inversion process because of the proximity of the benzene ring to the methyl groups, which suppresses the *cis*-to-*trans* thermal isomerization.[16]

The change in fluorescence intensity also reflects the distinct thermal relaxation processes of the two azo compounds. Spectral tracing in Fig. 3b shows that BDMAB had a much slower fluorescence decrease in the dark than BMAB. This is consistent with the concept that *ortho*-dimethylation retards the *cis*-to-*trans* thermal isomerization rate, thereby retaining the fluorescence intensity for a longer period. Several reports have shown that *cis*-Az derivatives coupled with fluorophores that are thermally isomerized to the *trans* form are accompanied by a fluorescence-fading behavior. This is because the *trans*-isomers favor photoinduced electron transfer from the lone pair electrons on the azo group to the HOMO of excited fluorophores through effective π-conjugation (reductive electron transfer).[17] However, it is believed that the thermal-induced fluorescence quenching for BMAB and BDMAB that lack fluorophore coupling is primarily attributed to the dynamic molecular disassembly that occurs during *cis*-to-*trans* isomerization.
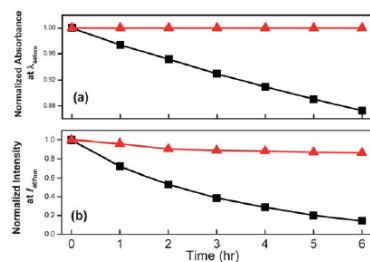
In summary, we successfully prepared blue-fluorescent *cis*-rich BMAB and BDMAB solutions upon UV light irradiation and demonstrated an unprecedented result of photoswitchable fluorescence "on/off" behavior for these two azo compounds. The change in emission intensity could be controlled by alternating UV and white light exposure within several minutes, which is also accompanied by a reversible *trans* ↔ *cis* photoisomerization. Although the reasons for the fluorescence enhancement and rapid photoswitchable behavior are not yet understood, it is proposed that the dynamic molecular assembly and disassembly processes during *trans* ↔ *cis* isomerization through external stimuli (*e.g.*, light and heat) was crucial to this unusual phenomenon. Moreover, compared with BMAB, BDMAB composed of two methyl groups on the *ortho* position showed extremely slow thermal *cis*-to-*trans* isomerization and a stable fluorescence expression in the dark for a longer period. This steady emission allows *cis*-BDMAB to be maintained in the fluorescent "on" state at ambient temperature toward the fields of molecular sensing and imaging with spatiotemporal concerns until we switch off the fluorescence by visible light irradiation.

Notes and references

1 N. Tamai and H. Miyasaka, *Chem. Rev.*, 2000, **100**, 1875.
2 T. Ikeda and T. Ube, *Mater. Today*, 2011, **14**, 480; J. Garcia-Amorós, S. Nonell and D. Velasco, *Chem. Commun.*, 2011, **47**, 4022; J. Garcia-Amorós, S. Nonell and D. Velasco, *Chem. Commun.*, 2012, **48**, 3421.
3 V. K. S. Hsiao and C. Y. Ko, *Opt. Express*, 2008, **16**, 12670; V. K. S. Hsiao, Y. B. Zheng, B. K. Juluri and T. J. Huang, *Adv. Mater.*, 2008, **20**, 3528; U. A. Hrozhyk, S. V. Serak, N. V. Tabiryan, T. J. White and T. J. Bunning, *Opt. Express*, 2010, **18**, 9653; M. H. Wu, C. C. Chu, M. C. Cheng and V. K. S. Hsiao, *Mol. Cryst. Liq. Cryst.*, 2012, **557**, 176.
4 H. Rau, *Angew. Chem., Int. Ed. Engl.*, 1972, **12**, 224; C. G. Morgante and W. S. Struve, *Chem. Phys. Lett.*, 1979, **68**, 267.
5 M. Han and M. Hara, *J. Am. Chem. Soc.*, 2005, **127**, 10951; M. R. Han, Y. Hirayama and M. Hara, *Chem. Mater.*, 2006, **18**, 2784.
6 M. Han, Y. Norikane, K. Onda, Y. Matsuzawa, M. Yoshida and M. Hara, *New J. Chem.*, 2010, **34**, 2892.
7 M. Shimomura and T. Kunitake, *J. Am. Chem. Soc.*, 1987, **109**, 5175.
8 C. Y. Hsu and Y. L. Liu, *Chem.–Eur. J.*, 2011, **17**, 5522.
9 O. Tsutsumi, T. Shiono, T. Ikeda and G. Galli, *J. Phys. Chem. B*, 1997, **101**, 1332; J. Azuma, N. Tamai, A. Shishido and T. Ikeda, *Chem. Phys. Lett.*, 1998, **288**, 77; J. H. Sung, S. Hirano, O. Tsutsumi, A. Kanazawa, T. Shiono and T. Ikeda, *Chem. Mater.*, 2002, **14**, 385.
10 N. J. Bunce, G. Ferguson, C. L. Forber and G. J. Stachnyk, *J. Org. Chem.*, 1987, **52**, 394; M. Han, T. Honda, D. Ishikawa, E. Ito, M. Hara and Y. Norikane, *J. Mater. Chem.*, 2011, **21**, 4696.
11 H. Nishioka, X. Liang, H. kashida and H. Asanuma, *Chem. Commun.*, 2007, 4354.
12 M. R. Han, D. Hashizume and M. Hara, *New J. Chem.*, 2007, **31**, 1746.
13 $\Phi_f = \Phi_s(A_s In^2/AI_s n_s^2)$, where Φ_f, *A*, *I*, and *n* are the quantum yield, absorbance, integrated fluorescence intensity, and refractive index, respectively. The 's' subscript refers to the standard, 9,10-diphenylanthracene.
14 T. Asano and T. Okada, *J. Org. Chem.*, 1986, **51**, 4454; J. Garcia-Amorós, M. Martínez, H. Finkelmann and D. Velasco, *J. Phys. Chem. B*, 2010, **114**, 1287.
15 The first-order rate constant (*k*) was determined by fitting the experimental data to the equation: $\ln[(A_t - A_\infty)/(A_0 - A_\infty)] = -kt$,

Fig. 3 The change in (a) absorbance and (b) fluorescence intensity for *cis*-to-*trans* thermal isomerization. BMAB (■), BDMAB (▲).

where A_t, A_0, and A_∞ are the absorbance at 445 nm at time t, time zero, and infinite time, respectively.

16 A. A. Beharry, O. Sadovski and G. A. Woolley, *J. Am. Chem. Soc.*, 2011, **133**, 19684; A. A. Beharry and G. A. Woolley, *Chem. Soc. Rev.*, 2011, **40**, 4422.

17 P. S. Zacharias, S. Ameerunisha and S. R. Korupoju, *J. Chem. Soc., Perkin Trans. 2*, 1998, 2055; Y. Li, N. Zhou, W. Zhang, F. Zhang, J. Zhu, Z. Zhang, Z. Cheng, Y. Tu and X. Zhu, *J. Polym. Sci., Part A: Polym. Chem.*, 2011, **49**, 4911.

This journal is © The Royal Society of Chemistry 2012

J. Mater. Chem., 2012, **22**, 20874–20877 | 20877

Reference 3

PAPER

Light-induced spectral shifting generated from azo-dye doped holographic 2D gratings

Yan Jun Liu,[a] Yu-Chuan Su,[b] Yu-Jui Hsu[b] and Vincent K. S. Hsiao[*b]

Optically tunable two-dimensional (2D) gratings were holographically fabricated in azobenzene-doped polymer-dispersed liquid crystals (LCs) using a single diffractive element. Our experiments showed that the diffraction efficiency of the gratings could be switched reversibly upon light irradiation. More importantly, we demonstrated for the first time that the diffractive spectrum from the holographic 2D gratings could be optically tuned by about 24 nm, which might be useful for optically switchable filters and spectroscopic applications. The dynamic switching is attributed to the changes of refractive index modulation between LC-rich and polymer-rich areas due to the *trans–cis*-isomerization-triggered nematic–isotropic phase transition of liquid crystals. In addition, our 2D holographic gratings have polarization-insensitive optical properties for normally incident light. The all-optical tuning behavior is highly reversible and reproducible, making this kind of grating promising in active photonic elements.

Introduction

Light responsive materials are promising candidates for all-optically addressable devices. All-optical control is advantageous since it leverages the benefits of light directed effects—remote, temporal, and spatial control. In the framework of all-optical control, azobenzenes and their derivatives are the most common photoswitchable materials to realize all-optically controllable devices. The reversible *trans–cis* isomerization of azobenzene derivatives by photoirradiation is the root of all-optical control,[1–10] which subsequently results in significant changes of optical properties. Azobenzenes and nematic liquid crystals (LCs) can be mixed together to form a host–guest photo-responsive material system. The photoisomerization of the guest molecules can be used to directly influence the order parameter or isothermally induce the nematic–isotropic phase transition of the host LC system.[11,12]

Holographic polymer-dispersed liquid crystal (H-PDLC)[13] is a well-known photolithographic technique that utilizes a holographic interference patterning onto the LC–prepolymer mixture syrup for fabricating various photonic elements. It offers many advantages including single-step fabrication, unique electro-optical properties, and fast responses. Thus far, many one-, two-, and three-dimensional (1-, 2-, and 3D) photonic structures have been demonstrated using H-PDLC materials.[14–21] LCs exist in a form of droplets of nanoscale size (less than 100 nm) in those

holographically fabricated periodic structures. Owing to the high surface-area-to-volume ratio of nanoscale LC droplets, a high electric field (10–20 V μm⁻¹) is often required to drive H-PDLC devices.[22–24] However, the all-organic nature of H-PDLC devices makes them vulnerable to high electric fields and thereby fore-stalls practical applications. Therefore, alternative approaches to drive the H-PDLC devices are being intensively explored.

In this paper, we report for the first time that the diffractive spectrum from the holographic 2D gratings, fabricated using only a single diffraction element, a photomask, could be optically tuned about 24 nm. By doping a photochromic dye (azobenzene) into the H-PDLC materials, the resulting gratings possess all-optically tunable transmission and diffraction properties. We have characterized their photoresponsive optical properties and analyzed the underlying physical mechanism in details. This all-optical tuning behavior makes this type of grating promising for many active photonic elements, such as optical switches, spatial light modulators, switchable add/drop filters, and spectroscopic applications.

Experimental

The starting prepolymer mixture syrup consisted of 60 wt% monomer, dipentaerythritol penta-/hexa-acrylate (DPHPA), 7 wt% cross-linking monomer, *N*-vinylpyrrolidone (NVP), 1 wt% photoinitiator, rose bengal (RB), and 2 wt% coinitiator, *N*-phenylglycine (NPG), all from Sigma-Aldrich. The photoresponsive material system was a homogeneous mixture of 15 wt% BMAB (4-butyl-4′-methyl-azobenzene) and 85 wt% nematic LC, MDA3461, from Merck (Taiwan Branch). The composition of 30% LC in the LC–prepolymer mixture syrup is the optimized condition in our experiment. The MDA3461 liquid crystal has an

ªInstitute of Materials Research and Engineering, Agency for Science, Technology and Research (A*STAR), 3 Research Link, Singapore 117602, Singapore
ᵇDepartment of Applied Materials and Optoelectronic Engineering, National Chi Nan University, No. 1, University Rd., Puli, NanTou, 54561, Taiwan. E-mail: kshsiao@ncnu.edu.tw
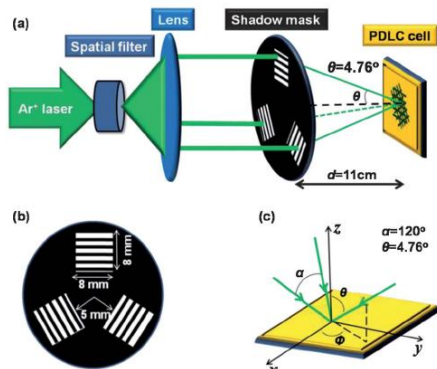
This journal is © The Royal Society of Chemistry 2012

J. Mater. Chem., 2012, **22**, 14191–14195 | 14191

Fig. 1 The schematic of the optical setup (a), specially designed mask (b), and interference configuration of three first-order diffracted beams from the mask (c).

ordinary refractive index (RI) of $n_o = 1.514$ and a birefringence of $\Delta n = 0.258$. Grating sample cells were prepared by placing 15 µL of LC–prepolymer mixture between two glass slides. The thickness of the grating sample was ~3 µm.

The optical setup for the fabrication is schematically illustrated in Fig. 1(a). A photomask was used to create a three-beam interference pattern. The mask consists of three diffraction gratings arranged at 120° relative to one another. In our experiment, each grating on the mask has an area of 8×8 mm² and the grating period is 6 µm. Fig. 1(b) and (c) show the schematic of the mask and three diffracted beams. This single mask implementation improves the alignment and stability of the optical setup, making it more robust than the multiple beam setups reported previously. An Ar⁺ laser operating at 514.5 nm with pumping power ~100 mW cm⁻² was used to generate the diffraction pattern. When a cell filled with the LC–prepolymer mixture is exposed to the diffraction pattern under pumping power ~10 mW cm⁻² for 6 min, the LC and polymer will redistribute due to the polymerization of the prepolymer induced by the light, thus forming a 2D structure inside the cell. It is worth mentioning that the light for holographic patterning in our experiment can induce the *cis–trans* isomerization of the BMAB molecules, hence making most BMAB molecules exist in the *trans* state and facilitating the alignment of the LC molecules.

Results and discussion

The electrical field distribution of a multi-beam interferences can generally be described by

$$I(\mathbf{r}) = \left[\sum_{j=1}^{n} \mathbf{E}_j(\mathbf{r}) \exp\left(i\mathbf{k}\cdot\mathbf{r} + i\phi_j \right) \right] \left[\sum_{j=1}^{n} \mathbf{E}_j^*(\mathbf{r}) \exp\left(- i\mathbf{k}\cdot\mathbf{r} - i\phi_j \right) \right]$$
$$= \sum_{j=1}^{n} |\mathbf{E}_j|^2 + \sum_{i \neq j}^{n} \mathbf{E}_i \cdot \mathbf{E}_j^* \exp\left[i(\mathbf{k}_i - \mathbf{k}_j)\cdot\mathbf{r} + i\phi_{ij} \right]$$

$$(1)$$

where, $\mathbf{E}$ is the amplitude, $\mathbf{k}$ is the wave vector, i and j are positive integers, ϕ_{ij} is the initial phase difference between two incident waves, and $\mathbf{r}$ is the position vector. As reported before, all 14 Bravais lattices can be fabricated by recording 4 plane wave interference fringes.[25] In our experiment, the beam vectors of the three diffracted first-order beams can be written as

$$\hat{\mathbf{k}}_1 = \sin\theta\cos\varphi_1\hat{e}_x + \sin\theta\sin\varphi_1\hat{e}_y + \cos\theta\hat{e}_z \qquad (2)$$

$$\hat{\mathbf{k}}_2 = \sin\theta\cos\varphi_2\hat{e}_x + \sin\theta\sin\varphi_2\hat{e}_y + \cos\theta\hat{e}_z \qquad (3)$$

$$\hat{\mathbf{k}}_3 = \sin\theta\cos\varphi_3\hat{e}_x + \sin\theta\sin\varphi_3\hat{e}_y + \cos\theta\hat{e}_z \qquad (4)$$

where is a unit wave vector, $\hat{e}$ is a unit coordinate vector, θ is the angle between the diffracted laser beam and the z-axis (the first order diffraction angle), and φ is the angle between the projection of the laser beam on the x–y plane and x-axis [Fig. 1(c)]. Substituting (2)–(4) into (1) with $\theta = 4.76°$, $\varphi_1 = 180°$, $\varphi_2 = -60°$, and $\varphi_3 = 60°$, we have

$$I = (\mathbf{E}_1 + \mathbf{E}_2 + \mathbf{E}_3)\cdot(\mathbf{E}_1 + \mathbf{E}_2 + \mathbf{E}_3)^*$$
$$= |\mathbf{E}_1|^2 + |\mathbf{E}_2|^2 + |\mathbf{E}_3|^2$$
$$+ 2\mathbf{E}_1\cdot\mathbf{E}_2\cos\left(-\frac{3}{2}kx\sin\theta + \frac{\sqrt{3}}{2}ky\sin\theta \right)$$
$$+ 2\mathbf{E}_1\cdot\mathbf{E}_3\cos\left(-\frac{3}{2}kx\sin\theta - \frac{\sqrt{3}}{2}ky\sin\theta \right) \qquad (5)$$
$$+ 2\mathbf{E}_2\cdot\mathbf{E}_3\cos\left(\sqrt{3}ky\sin\theta \right)$$

The simulated 3D interference pattern assuming the same intensity for the three first-order diffracted beams is shown in Fig. 2(a). It is worth mentioning that the period of this triangular lattice equals two thirds of the diffraction grating period, *i.e.*, 4 µm, which does not depend on the wavelength of light.[26]

Fig. 2(b) and (c) are the optical images of a 2D H-PDLC grating observed under a polarized optical microscope (POM) before and after removal of LCs. They reveal a clear hexagonal morphology with a lattice constant of about 3.82 µm, which is in good agreement with the simulation pattern [Fig. 2(a)], considering the general 5–10% volume shrinkage for the acrylate monomer during the photoinduced polymerization.[14] The diffraction patterns of the H-PDLC grating were checked to
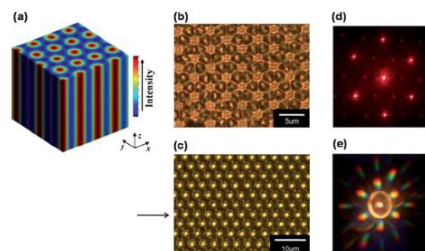

Fig. 2 (a) Simulated 3D interference pattern; observed morphologies of the H-PDLC grating under a POM before (b) and after (c) removal of the LCs; diffraction pattern for a normally incident He–Ne laser beam (d) and a collimated broadband white beam (e).

confirm the quasi-crystal structure. Fig. 2(d) and (e) show the visible diffraction patterns produced by a normally incident He–Ne laser beam operating at 633 nm and by a collimated broadband white beam, respectively, for our H-PDLC grating sample before the LC removal. The images clearly reveal the presence of quasiperiodicity within the sample. The observed points are sharp and symmetrically distributed. As reported by Gorkhali et al.,[27] all diffraction points in the first and higher orders should show an N-fold symmetry and have $2N$ diffracted points, where N is the number of interference beams used to produce the photonic structures. For our case, $N = 3$, in good agreement with the prediction, we can clearly see a 3-fold symmetry and 6 diffracted points for the same order of diffracted beams.

Fig. 3 shows the incident-angle-dependent transmission spectra. At normal incidence, the H-PDLC grating demonstrates a broad trough between 550 nm and 900 nm with the minimum transmission at 660 nm, which arises from the diffraction of the holographic 2D grating. By increasing the incident angle, the trough undergoes a blue shift and becomes broader. In addition, the minimum transmission of the trough reduces, indicating stronger diffraction. The angle dependent dispersion makes our fabricated 2D grating potentially useful for spectroscopic purposes.

Azobenzene-based optical materials have the distinct advantage that they can be optically controlled, which is an important factor for the future development of all-optical devices. Therefore, we investigated the dynamic changes in spectral transmission for the photoresponsive 2D grating structures. In our experiments, a violet laser (405 nm) and a green laser (532 nm)[28] were used to trigger the *trans–cis* and *cis–trans* isomerizations, respectively. Fig. 4 shows the typical dynamic changes in the spectral transmission at normal incidence for a fabricated sample under the violet laser irradiation with different intensities at a fixed irradiating angle of 45° to sample normal. With the increase of the irradiated intensity, the transmission trough blue-shifts by about 24 nm. We also investigated the optically switchable properties of the first-order diffracted light spectrum for the fabricated 2D grating structure (Fig. 5) using a spectrometer (Ocean Optics HR4000). Before light irradiation, the diffracted light shows a lesser amount of red light and that is the reason for the 600–650 nm dip [Fig. 5(a)]. Under light irradiation, the diffracted light intensity within the red regions increases [Fig. 5(b)], due to the enhancement of the diffraction ability of the grating
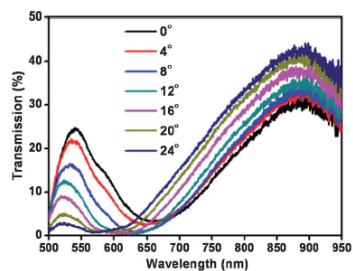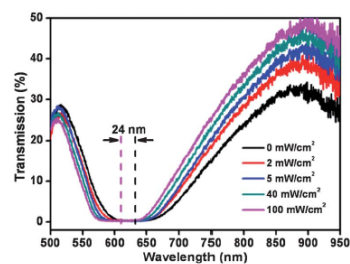

Fig. 4 Dynamic changes of transmission curve at normal incidence for a fabricated sample under various intensities emitting from a 405 nm laser diode.

sample. From Fig. 4 and 5, we conclude that our fabricated 2D grating samples could be used not only as an all-optically tunable filter but also as an all-optically tunable light source for spectrometric purposes.

Fig. 6 shows the time-dependent response of the 2D gratings under alternating laser pumping of two different wavelengths. The switching-on time, which corresponded to the decrease of
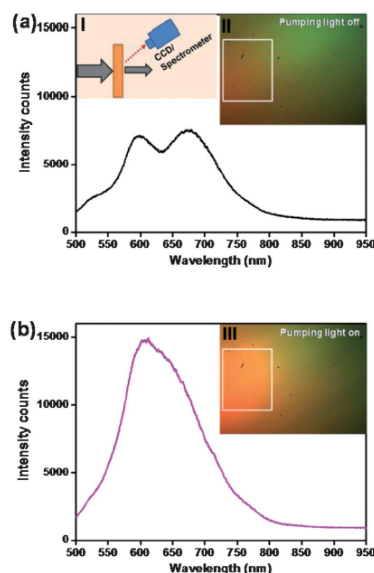

Fig. 5 Comparison of the first-order diffraction spectrum before (a) and after (b) 40 mW cm^{-2} 405 nm laser light irradiation. Inset I shows the schematic setup that uses a CCD or spectrometer to detect the color or spectrum change of the first-order diffraction. Insets II and III show the CCD-captured intensity changes before and after light irradiation (regions indicated by the white lines).
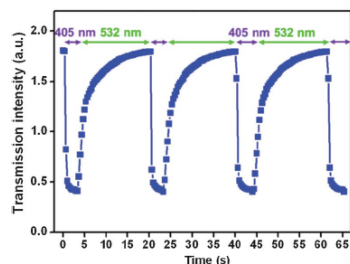

Fig. 3 Angle-dependent transmission spectra for a fabricated 2D grating.

This journal is © The Royal Society of Chemistry 2012

J. Mater. Chem., 2012, 22, 14191–14195 | 14193

Fig. 6 Photoresponses of the optically tunable H-PDLC gratings under the alternating violet (405 nm) and green (532 nm) laser irradiation. The laser intensity was 40 and 15 mW cm^{-2}, respectively. The processes of violet and green laser irradiation are shown in purple and green, respectively.

diffraction efficiency under 405 nm laser irradiation, was about 4 s, and the switching-off time, which corresponded to the increase of diffraction efficiency under 532 nm laser irradiation, was about 15 s.

The all-optically tunable behavior observed in our experiments could be attributed to the *trans–cis* isomerization-induced nematic–isotropic (N–I) phase change of the LCs. In our H-PDLC grating structures, LC-rich cylindrical arrays are formed and embedded inside the polymer matrices. The cross-linking polymerization of the monomers is accompanied by a contraction of the composites, known as polymerization shrinkage.[14] When the polymeric network shrinks, the LC droplets are compressed, and the rod-shaped LC molecules align along the long symmetric axis of the droplet (a preferential direction). In the case of two-dimensional gratings, liquid crystal cylinders are generally formed. Therefore, LC molecules form homeotropic alignment (*i.e.*, parallel to the polymer wall), as shown in Fig. 7(a). This kind of alignment and polarization insensitivity was also predicted by a previous report.[29] At this alignment state, the probe light, regardless of its polarization, experiences an effective RI, n_{eff}, of the LC region equal to the ordinary RI, n_o, of the LCs, *i.e.*, $n_{eff} = n_o = 1.514$. Only when the RI of polymer is exactly equal to that of LCs at homeotropic alignment can
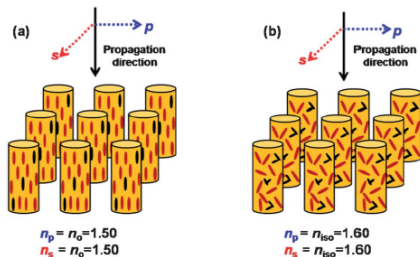
complete darkness of the 2D grating be observed under crossed polarizers. However, in practice, the refractive indices of polymer and LCs are not totally the same. The practical value for the cured polymer is about 1.529,[30] which is slightly different from that of LCs. Such a difference in RI will cause sufficient phase retardation, hence inducing obvious contrast in the brightness, as observed in Fig. 2. Upon the violet photoirradiation, the azo-LC molecules absorb the violet light and then transform from *trans* to *cis*, inducing the N–I phase transition of the LCs, as shown in Fig. 7(b). The empirical effective index for an isotropic LC can be estimated as $n_{iso} \cong (2n_o + n_e)/3$. For the LC MDA3461 used in our experiment, this value is $n_{iso} = 1.60$. At the isotropic state, $n_{eff} = n_{iso} = 1.60$. Note that the RI of polymer is unaltered after violet light irradiation, $n_{poly} = 1.5$. Therefore, the index modulation, Δn, between the LC-rich and polymer-rich regions inside the 2D grating structure increases when the N–I phase transition of the LCs occurs. On the other hand, our 2D gratings can simply be considered as three multiplexed gratings with a 60° intersecting angle. For a grating, the magnitude of the diffraction efficiency strongly depends on the diffraction regime determined by the parameter $Q = 2\pi\lambda L/n_o\Lambda^2$, where λ is the visible wavelength, Λ is the grating period ($\sim$4 μm), L is the film thickness ($\sim$3 μm), and n_o is the average RI. Here, n_o is estimated to be $\sim$1.55 from the ratio of LC and polymer molecules in the PDLC. The parameter Q is calculated to be <1. As a result, the fabricated grating works in the Raman-Nath regime. The first-order diffraction efficiency is therefore given by $\eta = J_1^2(2\pi\Delta n/\lambda)$ where J_1 is the first-order Bessel function of the first kind. Intuitive calculations from the equation show that the diffraction efficiency for the shorter wavelengths increases exponentially faster
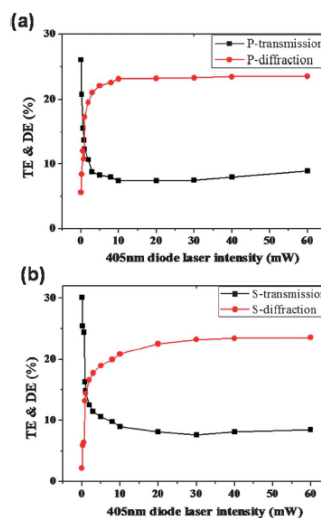

Fig. 7 The proposed model for the alignment of LC molecules inside the cylindrical polymeric cavities before and after light pump.

Fig. 8 Changes of transmission and diffraction as a function of irradiated laser intensity for both p- and s-polarized probe light.

14194 | *J. Mater. Chem.*, 2012, **22**, 14191–14195

This journal is © The Royal Society of Chemistry 2012

than that for the longer wavelengths. As a result, we observed an increase of the diffraction intensity. More importantly, the larger increase in the diffraction efficiency for shorter wavelengths than for longer wavelengths leads to a blue shift as the RI modulation, Δn, increases.

From the above discussion, another distinct advantage of our H-PDLC gratings is that they show polarization-independent optical behavior in both transmission and diffraction at the normal incidence, which is important for many optical devices that require polarization-insensitive operation. As a further confirmation, the polarization-dependent transmission and diffraction were measured as a function of pumping intensity. The results are shown in Fig. 8. From Fig. 8(a) and (b), it can be seen that both p- and s-polarized light show very similar dynamic behavior in both transmission and diffraction. More importantly, there are only slight differences in the TE and DE values for both p- and s-polarized light, which experimentally confirms that our 2D gratings have polarization-insensitive optical properties for normally incident light.

Conclusion

We have demonstrated, for the first time, the light-induced spectral shifting from a 2D grating fabricated by a photolithographic technique that utilizes a holographic interference pattern. This method offers simple, single-step, and low-cost fabrication compared to conventional lithography. Upon light irradiation, the diffraction of the 2D gratings was switched reversibly. The physical mechanism for the switching effect was the *trans–cis*-isomerization-induced N–I phase change of the LCs. Our holographic 2D gratings have also demonstrated polarization-insensitive optical properties for normally incident light. The demonstrated optically tunable 2D diffractive photonic structures are potentially useful for many active photonic elements, such as optical switches, spatial light modulators, switchable add/drop filters, and spectroscopic applications.
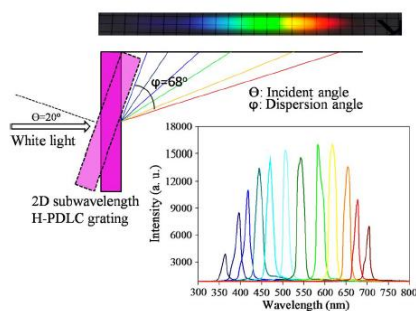
Acknowledgements

Notes and references

1 A. Urbas, J. Klosterman, V. Tondiglia, L. Natarajan, R. Sutherland, O. Tsutsumi, T. Ikeda and T. Bunning, *Adv. Mater.*, 2004, **16**, 1453.
2 S. Huang, S. Wu and A. Y. Fuh, *Appl. Phys. Lett.*, 2006, **88**, 041104.
3 U. A. Hrozhyk, S. V. Serak, N. V. Tabiryan and T. J. Bunning, *Adv. Mater.*, 2007, **19**, 3244–3247.
4 L. De Sio, A. Veltri, C. Umeton, S. Serak and N. Tabiryan, *Appl. Phys. Lett.*, 2008, **93**, 181115.
5 V. K. S. Hsiao and W.-T. Chang, *Appl. Phys. B: Lasers Opt.*, 2010, **100**, 539–546.
6 Y.-C. Su, C.-C. Chu, W.-T. Chang and V. K. S. Hsiao, *Opt. Mater.*, 2011, **34**, 251–255.
7 Y. J. Liu, H. T. Dai and X. W. Sun, *J. Mater. Chem.*, 2011, **21**, 2982–2986.
8 N. Kawatsuki and Emi Uchida, *Appl. Phys. Lett.*, 2003, **83**, 1560–1562.
9 R. A. van Delden, T. Mecca, C. Rosini and B. L. Feringa, *Chem.–Eur. J.*, 2004, **10**, 61–70.
10 M.-H. Wu, C.-C. Chu, M.-C. Cheng and V. K. S. Hsiao, *Mol. Cryst. Liq. Cryst.*, 2012, **557**, 176–189.
11 K. Ichimura, *Chem. Rev.*, 2000, **100**, 1847–1873.
12 Y. J. Liu, Y. B. Zheng, J. Shi, H. Huang, T. R. Walker and T. J. Huang, *Opt. Lett.*, 2009, **34**, 2351–2353.
13 T. J. Bunning, L. V. Natarajan, V. P. Tondiglia and R. L. Sutherland, *Annu. Rev. Mater. Sci.*, 2000, **30**, 83–115.
14 R. L. Sutherland, L. V. Natarajan, V. P. Tondiglia and T. J. Bunning, *Chem. Mater.*, 1993, **5**, 1533–1538.
15 M. J. Escuti, J. Qi and G. P. Crawford, *Appl. Phys. Lett.*, 2003, **83**, 1331–1333.
16 R. L. Sutherland, V. P. Tondiglia, L. V. Natarajan, S. Chandra, D. Tomlin and T. J. Bunning, *Opt. Express*, 2002, **10**, 1074–1082.
17 V. P. Tondiglia, L. V. Natarajan, R. L. Sutherland, D. Tomlin and T. J. Bunning, *Adv. Mater.*, 2002, **14**, 187–191.
18 M. J. Escuti and G. P. Crawford, *Opt. Eng.*, 2004, **43**, 1973–1987.
19 Y. J. Liu and X. W. Sun, *Appl. Phys. Lett.*, 2006, **89**, 171101.
20 Y. J. Liu and X. W. Sun, *Jpn. J. Appl. Phys.*, 2007, **46**, 6634–6638.
21 Y. J. Liu, H. T. Dai, E. S. P. Leong, J. H. Teng and X. W. Sun, *Appl. Phys. B: Lasers Opt.*, 2011, **104**, 659–663.
22 Y.-H. Fan, Y.-H. Lin, H. Ren, S. Gauza and S.-T. Wu, *Appl. Phys. Lett.*, 2004, **84**, 1233–1235.
23 Y. J. Liu, X. W. Sun, H. T. Dai, J. H. Liu and K. S. Xu, *Opt. Mater.*, 2005, **27**, 1451–1455.
24 Y. J. Liu, X. W. Sun, J. H. Liu, H. T. Dai and K. S. Xu, *Appl. Phys. Lett.*, 2005, **86**, 041115.
25 L. Z. Cai, X. L. Yang and Y. R. Wang, *J. Opt. Soc. Am. A*, 2002, **19**, 2238–2244.
26 V. Berger, O. Gauthier-Lafaye and E. Costard, *Electron. Lett.*, 1997, **33**, 425–426.
27 S. P. Gorkhali, J. Qi and G. P. Crawford, *J. Opt. Soc. Am. B*, 2006, **23**, 149–158.
28 A. Urbas, V. Tondiglia, L. Natarajan, R. Sutherland, H. Yu, J.-H. Li and T. Bunning, *J. Am. Chem. Soc.*, 2004, **126**, 13580–13581.
29 P. Kossyrev, M. E. Sousa and G. P. Crawford, *Adv. Funct. Mater.*, 2004, **14**, 1227–1232.
30 Y. J. Liu, B. Zhang, Y. Jia and K. S. Xu, *Opt. Commun.*, 2003, **218**, 27–32.

Reference 4

Open Access

Large-Angle Color Dispersion Based on 2-D Hexagonal Subwavelength Holographic Gratings

Ya-Yun Lo
Jianhui Yu
Yu-Chuan Su
Vincent K. S. Hsiao
Zhe Chen

IEEE

Large-Angle Color Dispersion Based on 2-D Hexagonal Subwavelength Holographic Gratings

Ya-Yun Lo,[1] Jianhui Yu,[2] Yu-Chuan Su,[1] Vincent K. S. Hsiao,[1] and Zhe Chen[2]

[1] Department of Applied Materials and Optoelectronic Engineering,
National Chi Nan University, Nantou 54561, Taiwan
[2] Key Laboratory of Optoelectronic Information and Sensing Technologies of Guangdong Higher
Educational Institutes, Jinan University, Guangzhou 510632, China

Abstract: This paper presents large-angle color dispersion using a holographically fabricated 2-D subwavelength transmission grating. A dispersion angle of 68° is observed within continuous spectrum dispersion from 360 to 700 nm at an incident angle of 20° using white light as a probe beam. By changing the angle between the sample normal and the probe beam, the dispersed spectrum can be tuned at a spectral resolution of 3.6 nm per degree.

Index Terms: Subwavelength structures, diffractive optics.

1. Introduction

A diffraction grating acts as a prism and disperses different wavelengths of light into a spectrum. The grating spacing or groove determines the dispersion angle. Using a commercial replicated holographic grating of 2400 grooves/mm (dispersion = 0.33 nm/mrad) as an example, the dispersion angle from a light wavelength of 400 to 700 nm is 52°. Recently, numerous studies have focused on using photonic crystal structures to create a large-angle light dispersion phenomenon [1]–[12]. They have reported a maxima dispersion angle of approximately 50° [13].

This paper presents a 68° white-light dispersion angle (360 to 700 nm) using 2-D subwavelength gratings. The hexagonal gratings of a 500-nm period were fabricated using a holographic polymer-dispersed liquid crystal (H-PDLC) technique that used a single prism as an optical interference setup [14]. Typically, H-PDLC gratings do not provide sufficient refractive index (RI) contrast when fabricating 2-D or 3-D subwavelength periodic structures. However, adding a moderate amount of solvent increases the RI contrast to 0.2 because of the RI difference between the polymer and nanopore regions [15]. The results of this paper offer alternatives for fabricating low-cost efficient optical components used for spectroscopic purposes.

2. Experiment

Fig. 1 shows the optical setup for the holographically fabricated samples. A specially designed prism was used to achieve three-beam interference from single laser exposure. A description of the specially designed prism and corresponding interference patterning technique can be found in [14].
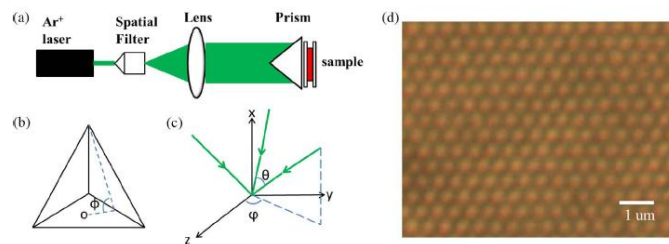
Fig. 1. Diagrams of (a) the optical setup, (b) the specially designed prism ($\phi = 60°$), and (c) the three beam interference angle ($\theta = 25.3°$ and $\varphi = 60°$) created by single writing laser exposure. (d) Dark-field optical image of the fabricated 2-D hexagonal periodic structure.
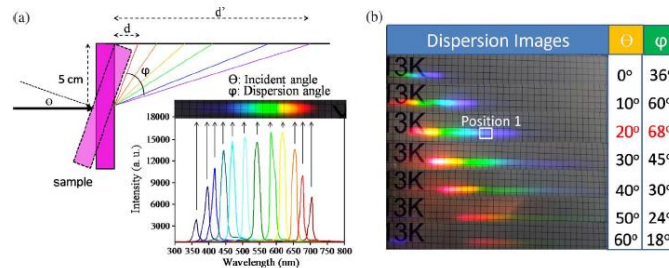

Fig. 2. (a) Experiment setup for measuring the white light dispersion angle using the 2-D subwavelength grating. (b) Color dispersion images from unpolarized white light (probe beam) recorded at different probe beam incident angles. The inset shows the dispersed spectra from 360 to 700 nm at different positions.

The holographic writing laser was expanded and collimated to 40 mm in diameter and exposed to the top of the prism. The 3-μm-thick sandwiched sample was placed on the bottom of the prism using index-matching oil. The prepolymer syrup consisted of 50-wt.% monomer, dipentaerythritolhydroxypenta acrylate; 20-wt.% toluene; 7-wt.% cross-linking monomer, N-vinylpyrrollidone; 1-wt.% photoinitiator, rose bengal; and 2-wt.% coinitiator, N-phenylglycine, procured from Sigma-Aldrich, and 20-wt.% nematic LC, MDA3461 procured from Merck (Taiwan). The sandwiched sample was exposed to a 514-nm-Ar+ laser for 3 min and cured under a table light for 24 h. During holographic interference patterning, the monomer fluids were cross-linked and became polymer in the high light-intensity regions; at the same time, the LC/toluene mixture were phase-separated in the low light-intensity regions. The sandwiched sample must be opened to allow the solvent vapor to evaporate to achieve optical characteristics. Fig. 1(d) shows an image of the fabricated structure under an optical microscope in dark-field operation mode. Dark-field operation enhances the image contrast between polymer (dark) and nanopore (bright) regions.

3. Results and Discussion

Fig. 2(a) shows the schematic setup for recording dispersion angles and spectra from the 2-D subwavelength transmission grating, and Fig. 2(b) shows the corresponding dispersion spectra images at different white-light incident angles (θ). The dispersion angle is calculated by measuring the dispersion distance (d) from 360 to 700 nm. The dispersion angle increases when the incident angle increases, reaching a maximal value of 68° at an incident angle of 20°. The dispersion angle
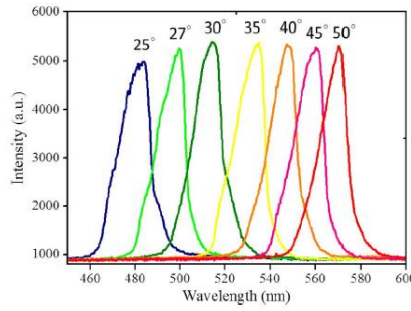
Fig. 3. Tunable dispersion spectra of 2-D subwavelength holographic transmission gratings dependent on the incident angle of unpolarized white light when the detector is fixed at position 1, as shown in Fig. 2(b).
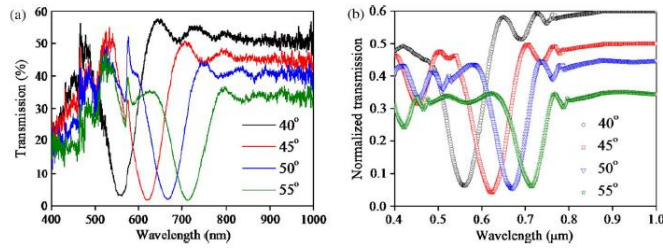

Fig. 4. (a) Measured transmittance responses and (b) simulated spectra for the 2-D hexagonal subwavelength transmission grating with different incident angles of s-polarized probe beam. The scattering loss was considered to be 40%, 50%, 55%, and 65% corresponded to rotating angle of 40°, 45°, 50°, and 55°.

decreases when the incident angle is larger than 20°, and the dispersed color vanishes when the incident angle is larger than 60°. This dispersion behavior is similar to that of commercial holographic gratings, where the dispersion angle increases with the incident angle and then decreases (see Fig. 3). The holographic transmission grating dispersion angle is calculated using the following equation:

$$\beta(\lambda) = \sin^{-1}\left(\frac{\lambda_i}{\Lambda} - \sin\alpha\right) \quad (1)$$

where $\beta(\lambda)$ is the dispersion angle corresponding to incident wavelength λ_i, α is the incident angle, and Λ is the grating period. Using a 1-D transmission grating with a period of 522 nm as an example, the calculated dispersion angles corresponding to 360 and 700 nm wavelengths are approximately 20° and 90°, respectively, at an incident angle of 20°. The calculated dispersion angle for a 1-D grating between 360 and 700 nm is 70°, which is similar to the proposed 2-D hexagonal grating.

Dispersion spectra shifts were recorded at Detector-Fixed Position 1 (see Fig. 2) by changing the probe beam incident angle. The peak position was tuned by 90 nm between a sample rotation of 25° and 50°, providing a spectral resolution of 3.6 nm per degree.

The transmission spectra for the sample at different probe beam incident angles were recorded and analyzed, as shown in Fig. 4. The experiment results in Fig. 4(a) and the simulated results in Fig. 4(b), obtained using DiffractMOD (RSoft Co.), show that the RI of the fabricated structure is 0.2, which is the same as that obtained from previously fabricated 1-D reflection gratings. A grating period of 522 nm was used in the simulation. By considering the scattering loss from the H-PDLC samples, the simulated results are matched to the experimental results.

4. Conclusion

This paper demonstrates large-angle color dispersion using a 2-D subwavelength holographic transmission grating. When an unpolarized white light is incident to the sample, a dispersion angle of 68° is observed within a continuous spectrum distributed from 360 to 700 nm. Rotating the sample tunes the detected spectrum and achieves a spectral resolution of 3.6 nm per degree. The results could be used for spectrometric applications. Future studies should investigate methods of tuning the spectrum without rotating the samples by adding or infiltrating photoactive molecules, such as azobenzene deriatives.

References

[1] H. Kosaka, T. Kawashima, A. Tomita, M. Notomi, T. Tamamura, T. Sato, and S. Kawakami, "Photonic crystals for micro lightwave circuits using wavelength-dependent angular beam steering," *Appl. Phys. Lett.*, vol. 74, no. 10, pp. 1370–1372, Mar. 1999.
[2] L. Wu, M. Mazilu, T. Karle, and T. F. Krauss, "Superprism phenomena in planar photonic crystals," *IEEE J. Quantum Electron.*, vol. 38, no. 7, pp. 915–918, Jul. 2002.
[3] T. Baba and T. Matsumoto, "Resolution of photonic crystal superprism," *Appl. Phys. Lett.*, vol. 81, no. 13, pp. 2325–2327, Sep. 2002.
[4] N. C. Panoiu, M. Bahl, and R. M. Osgood, Jr., "Optically tunable superprism effect in nonlinear photonic crystals," *Opt. Lett.*, vol. 28, no. 24, pp. 2503–2505, Dec. 2003.
[5] J. J. Baumberg, N. M. B. Perney, M. C. Netti, M. D. C. Charlton, M. Zoorob, and G. J. Parker, "Visible wavelength super-refraction in photonic crystal superprisms," *Appl. Phys. Lett.*, vol. 85, no. 3, pp. 354–356, Jul. 2004.
[6] A. Lupu, E. Cassan, S. Laval, L. El Melhaoui, P. Lyan, and J. M. Fedeli, "Experimental evidence for superprism phenomena in SOI photonic crystals," *Opt. Exp.*, vol. 12, no. 23, pp. 5690–5696, Nov. 2004.
[7] T. Matsumoto, S. Fujita, and T. Baba, "Wavelength demultiplexer consisting of Photonic crystal superprism and superlens," *Opt. Exp.*, vol. 13, no. 26, pp. 10768–10776, Dec. 2005.
[8] B. Momeni, J. Huang, M. Soltani, M. Askari, S. Mohammadi, M. Rakhshandehroo, and A. Adibi, "Compact wavelength demultiplexing using focusing negative index photonic crystal superprisms," *Opt. Exp.*, vol. 14, no. 6, pp. 2413–2422, Mar. 2006.
[9] D. Bernier, X. Le Roux, A. Lupu, D. Marris-Morini, L. Vivien, and E. Cassan, "Compact, low cross-talk CWDM demultiplexer using photonic crystal superprism," *Opt. Exp.*, vol. 16, no. 22, pp. 17209–17214, Oct. 2008.
[10] L. Wang, W. Jiang, X. Chen, L. Gu, J. Chen, and R. T. Chen, "Fabrication of polymer photonic crystal superprism structures using polydimethylsiloxane soft molds," *J. Appl. Phys.*, vol. 101, no. 11, pp. 114316-1–114316-6, Jun. 2007.
[11] J. Amet, G. Ulliac, F. I. Baida, and M.-P. Bernal, "Experimental evidence of enhanced electro-optic control on a lithium niobate photonic crystal superprism," *Appl. Phys. Lett.*, vol. 96, no. 10, pp. 103111-1–103111-3, Mar. 2010.
[12] M.-P. Bernal, J. Amet, J. Safioui, F. Devaux, M. Chauvet, J. Salvi, and F. I. Baida, "Pyroelectric control of the superprism effect in a lithium niobate photonic crystal in slow light configuration," *Appl. Phys. Lett.*, vol. 98, no. 7, pp. 071101-1–071101-3, Feb. 2011.
[13] M. S. Li, S. T. Wu, and A. Y.-G. Fuh, "Superprism phenomenon based on holographic polymer dispersed liquid crystal films," *Appl. Phys. Lett.*, vol. 88, no. 9, pp. 091109-1–091109-3, Feb. 2006.
[14] D. Luo, X. W. Sun, H. T. Dai, Y. J. Liu, H. Z. Yang, and W. Ji, "Two-directional lasing from a dye-doped two-dimensional hexagonal photonic crystal made of holographic polymer-dispersed liquid crystals," *Appl. Phys. Lett.*, vol. 95, no. 15, pp. 151115-1–151115-3, Oct. 2009.
[15] V. K. S. Hsiao, T. C. Lin, G. S. He, A. N. Cartwright, P. N. Prasad, L. V. Natarajan, V. P. Tondiglia, and T. J. Bunning, "Optical microfabrication of highly reflective volume Bragg gratings," *Appl. Phys. Lett.*, vol. 86, no. 13, pp. 131113-1–131113-3, Mar. 2005.

Reference 5

Dynamic Article Links ▶

COMMUNICATION

Reversibly light-modulated photoluminescence from azobenzene-impregnated porous silicon

Sheng-Lin Chen,[a] Chih-Chien Chu[bc] and Vincent K. S. Hsiao*[a]

Azobenzene-impregnated porous silicon (Azo-PS) was used, for the first time, as color-rewritable organic/inorganic hybrid material. Under UV light illumination, the generation of *cis*-Azo enhances the red photoluminescence (PL) emission.
10 **Images can be written and erased under external light and thermal stimulus.**

Canham's discovery of room-temperature photoluminescence (PL) from porous silicon (PS) made PS a promising luminescent material in 1990.[1] Over the last two decades, many researchers
15 have focused on enhancing the PL intensity of PS by laser annealing or tuning the PL spectrum from PS by impregnating organic or inorganic materials within the pores of the PS host.[2-13] However, those methods can only achieve passive tuning of the PL spectrum and intensity. Organic solvent and redox reaction
20 have been proved efficient to reversibly quenching the PL from PS.[14,15] However, the control of the amount of solvent vapors and redox species is not an easy task. Recent research has shown that azobenzene (Azo) derivatives can efficiently construct light-activated photonic materials or devices.[16-22] The *trans-cis*
25 photoisomerization of Azo modulates the wetting and desorption of surfaces, the pore geometry of porous materials, and the electrical and optical properties of organic and inorganic host materials.[16-22] This study shows, for the first time, that impregnating Azo into PS as an inorganic host can photoactively
30 tune the PL intensity and spectrum of PS. The PL spectral wavelength tuning range of 100 nm and the PL intensity of PS emission is tuned and switched under alternative UV and visible light illumination. The proposed system produces a flexible and functional organic/inorganic hybrid material capable of changing
35 its fluorescent emission in response to an external light stimulus.

The PS sample was prepared by anodic etching, where a p-type (10-100 Ω · cm) silicon substrate was placed in a homemade Telflon etching cell using a mixture of aqueous HF (purity 49%), isopropanol (IPA) and DI water, 1:2:1 by volume. The sample
40 was anodized at a current density of 50 mA/cm^2 for 30 min. No further chemical or thermal treatment was performed after etching. The freshly etched samples were impregnated with 2 µL of azobenzene molecules (4-butyl-4'-methoxyazobenzene) by capillary force. Suitable heating was applied to the Azo-PS
45 sample to maintain the homogeneous distribution of Azo

molecules within the PS. The PL spectra at room temperature were characterized with a 365 nm LED with a 50 mW/cm^{-1} excitation and fiber-based fluorescence spectrometer (USB 4000, Ocean Optics).
50   Figure 1 shows the PL spectra and PS corresponding images before and after Azo-impregnation. An ordinary red PL band, which can be efficiently electrically excited, appears in the freshly etched PS sample. The Azo-impregnation quenches the red band PL intensity. The quenching effect may be due to PL
55 from the PS being highly dependent on the interaction between physisorbed Azo molecules and the surface.[2]
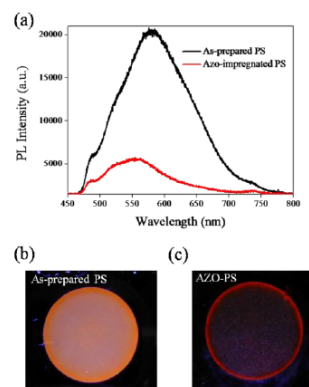

Fig. 1 (a) Room temperature PL from as-prepared PS and Azo-PS samples. Azo-impregnation severely quenches and slightly blueshifts the
60 red PL band originating on surface hydrides attached on the branches of the PS. (b) and (c) are images of the PS before and after Azo-impregnation, respectively. The PL excitation intensity in each case is 50 mW/cm^{-1} at 365 nm.

The Fourier transform infrared (FTIR) spectrum of freshly
65 etched PS, as shown in Fig. 2, presents a Si-H peak (at 2150 cm^{-1}), which contributes to the red emission PL. However, the Si-H group disappears after Azo-impregnation. Because these hydrides contribute to the red emission PL, this FTIR evidence suggests

that Azo-impregnation quenches the red band PL spectrum (Fig. 1a). The generation of O-H (at 3400 cm^{-1}) in the Azo-PS sample may produce another quenching effect. Other FTIR characteristics from the Azo-PS sample indicate the existence of a used azobenzene derivative.
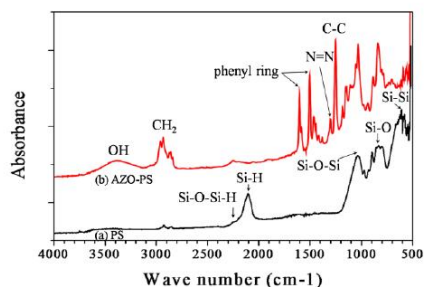

Fig. 2 FTIR spectra of (a) freshly etched PS and (b) Azo-impregnated PS. The surface Si-H group that contributes to the red PL emission disappears in the Azo-impregnated PS.

A new PL peak wavelength located at 650 nm increased its intensity under UV light illumination (Fig. 3a). Before UV light treatment, the sample shows less red. However, the PL emission spectrum redshifts, and the sample shows more red after UV light treatment. The PL intensity of the new peak located at 650 nm decreases under 532 nm laser light illumination. The PL intensity of the Azo-PS sample at 650 nm can be dynamically switched ON and OFF under alternative UV light and visible light illumination (Fig. 3b).

Previous studies involving the use of a liquid crystal (LC) to enhance the PL of LC-impregnated PS have indicated the possibility of energy transfer between LC and PS.[23,24] A photoinduced charge transfer between dye molecules and PS could also enhance and shift the PL spectrum.[3] Because the Azo molecule is a photochromic dye with a rod-like shape, it is likely to produce radiative and nonradiative energy transfers between impregnated Azo and PS. Furthermore, PS is extremely sensitive to environmental dielectrics.[2] At first, the rod-like Azo facilitates the impregnation of Azo into a cylindrical wall of pores. Therefore, the energy transfer between Azo and PS contributes to quenching and slightly blue-shifts the PL from Azo-PS (Fig. 1a). Under UV light illumination, subsequent *trans-cis* photoisomerization changes the value of the Azo dipole moment from 0 to 3.[25] The enhanced red hue of Azo-PS under UV illumination (Fig. 3) is due to rapid *trans-cis* isomerization, which causes a significant increase in the dipole moment of physisorbed Azo molecules. This variation in polarity with the surface and interface between Azo and PS can be dynamically switched by alternative UV and visible light, confirming the photoactive tuning of the PL emission from the Azo-PS sample.

The reversible change of the dipole moment induced by *trans-cis* photoisomerization from Azo molecules enables the writing and erasing of all types of photo patterned images under external stimuli. When the Azo-PS sample is exposed to UV light, red appears. The typical procedure of forming images on an Azo-PS

sample is to use a shadow mask and UV light exposure. Images can also be formed by exposing a UV-treated Azo-PS sample with a shadow mask and visible light exposure. In this situation, the visible light exposure areas have *trans*-Azo molecules, which show less red. The formatted images can be self-erased by keeping the UV light exposure, which makes all Azo become *cis*-Azo (all red). Alternatively, visible light exposure and heating the sample makes all Azo become trans-Azo (all less red), as Fig. 4 shows.
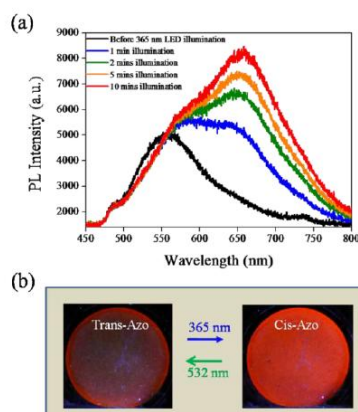

Fig. 3 (a) Temporal variation of the PL emission spectrum of the Azo-PS sample under UV light illumination. (b) is the image of the Azo-PS sample showing light-induced switching PL under alternative UV and visible light illumination. The PL excitation intensity in each case is 50 mW/cm^{-1} at 365 nm. The diameter of the etched PS is 15 mm.
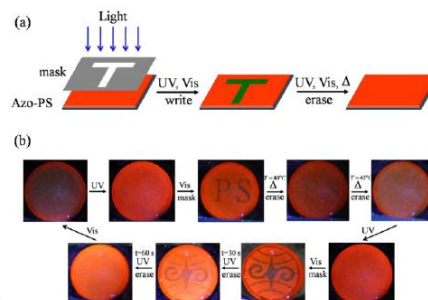

Fig. 4 Writing and erasing images on the Azo-PS sample. (a) Images created in Azo-PS by UV or visble light exposure through a shadow mask. The image in the Azo-PS sample self-erases under UV light (UV lamp, 365 nm, 6W, model UVL-56) within 3 mins. Exposure to a 10 mW/cm^2 532 nm laser for 10 s or heating the sample to approximately 45 °C for 30s erases the image on the Azo-PS sample. (b) PL images of rewritable Azo-PS sample under external stimuli. The sample was first exposed to a 50 mW/cm^{-1}, 365 nm LED light for 5 mins before writing a pattern on the Azo-PS sample using a 10 mW/cm^2 532 nm laser for 10s. Due to the *cis-trans* photoisomerization of the impregnated Azo, the red color vanishes and the image of mask is presented in the sample. Heating the sample

2 | *J. Mater. Chem. C*, [year], **[vol]**, 00–00

This journal is © The Royal Society of Chemistry [year]

erases the written pattern. Another pattern can be written using the same technique and erased by exposure to 50 mW/cm^{-1}, 365 nm LED light for 60 s. The diameter of the etched PS is 15 mm.

In conclusion, this study shows that impregnating Azo molecules into the pores of a PS host can photoactively tune and switch the room-temperature PL of PS. Under UV light illumination, the resulting increase in the dipole moment affects the radiative and nonradiative energy transfer between cis-Azo to PS host and enhances the red emission. This change in the PL spectrum is reversible and repeatable under alternative UV and visible light illumination. Future research should consider applying such system to phototunable photovoltaic devices based on PS materials.

Notes and references

^{a}Department of Applied Materials and Optoelectronic Engineering No. 1, University Rd., National Chi Nan University, Puli, NanTou, 54561, Taiwan; E-mail: kshsiao@ncnu.edu.tw
^{b}School of Applied Chemistry, Chung Shan Medical University, Taichung City 40201, Taiwan.
^{c}Department of Medical Education, Chung Shan Medical University Hospital, Taichung City 40201, Taiwan

1   A. G. Cullis and L.T. Canham, *Nature*, 1991, **353**, 335.
2   M. Lauerhaas and M. J. Sailor, *Science*, 1993, **261**, 1567.
3   L. T. Canham, *Appl. Phys. Lett.*, 1993, **63**, 337.
4   V. P. Parkhutik, R. D. Calleja, E. S. Matveeva and J. M. Martinez-Duart, *Synthetic Metals*, 1994, **67**, 111.
5   J. M. Rehma, G. L. McLendon, L. Tsybeskov and P. M. Fauchet, *Appl. Phys. Lett.*, 1995, **66**, 3669.
6   H. A. Lopez, X. L. Chen, S. A. Jenekhe and P. M. Fauchet, *J. Luminescence*, 1999, **80**, 115.
7   W. J. Salcedo, F. J. R. Fernandez and J. C. Rubim, *J Raman Spectrosc.*, 2001, **32**, 151.
8   H. Elhouichet and M. Oueslati, *Mater. Sci. Eng. B*, 2001, **79**, 27.
9   Y. Yamauchia, T. Sakuraia, Y. Hirohataa, T. Hinoa and M. Nishikawa, *Vacuum*, 2002, **66**, 415.
10   Y. Zhao, D. Yang, D. Li and M. Jiang, *Mater. Sci. Eng. B*, 2005, **116**, 95.
11   Y. Posada, L. F. Fonseca, P. Vallejo, L. San Miguel, O. Resto and I. Balberg, *J. Appl. Phys.*, 2006, **99**, 114313.
12   A. G. Palestino, M. B. de la Mora, J. A. del Río, C. Gergely and E. Pérez, *Appl. Phys. Lett.*, 2007, **91**, 3669.
13   M. Fakis, F. Zacharatos, V. Gianneta, P. Persephonis, V. Giannetas, and A. G. Nassiopoulou, *Mater. Sci. Eng. B*, 2009, **165**, 252.
14   J. M. Lauerhaas, G. M. Credo, J. L. Heinrich and M. J. Sailor, *J. Am. Chem. Soc.*, 1992, **114**, 1911.
15   B. Sciacca, S. Pace, P. Rivolo and F. Geobaldo, *Phys. Chem. Chem. Phys.*, 2012, **14**, 5251.
16   Y. Zhao and T. Ikeda, *Smart Light-Responsive Materials: Azobenzene-Containing Polymers and Liquid Crystals*, 2009, John Wiley & Sons, Hoboken, NJ.
17   M. -M. Russew and S. Hecht, *Adv. Mater.*, 2010, **22**, 3348.
18   R. Klajn, *Pure Appl. Chem.*, 2010, **82**, 2247.
19   N. Fuentes, A. Martin-Lasanta, L. Alvarez de Cienfuegos, M. Ribagorda, A. Parra and J. M. Cuerva, *Nanoscale*, 2011, **3**, 4003.
20   W. Feng, W. Luo and Y. Feng, *Nanoscale*, 2012, **4**, 6118.
21   Y. B. Zheng, B. K. Pathem, J. N. Hohman, J. C. Thomas, M. Kim and P. S. Weiss, *Adv. Mater.* 2013, **25**, 302.
22   L. Maggini, T. Marangoni, B. Georges, J. M. Malicka, K. Yoosa, A. Minoia, R. Lazzaroni, N. Armaroli and D. Bonifazi, *Nanoscale*, 2013, **5**, 634.
23   Yu. P. Piryatinski, L. O. Dolgov, O. V. Yaroshchuk and S. Lazarouk, *Mol. Cryst. Liq. Cryst.*, 2007, **467**, 195.
24   Q. Ma, R. Xiong and Y. Huang, *J. Luminescence*, 2011, **131**, 2053.
25   G. S. Hartley and R. J. W. Le Fevre, *J. Chem. Soc.* 1939, 531.